Palaeogeography, Palaeoclimatology, Palaeoecology xxx (xxxx) xxxx

Contents lists available at ScienceDirect

Palaeogeography, Palaeoclimatology, Palaeoecology

journal homepage: www.elsevier.com/locate/palaeo

Age and depositional environment of the Xiaheyan insect fauna, embedded in marine black shales (Early Pennsylvanian, China)

Steffen Trümper[a,b,**], Jörg W. Schneider[b,c], Tamara Nemyrovska[d], Dieter Korn[e], Ulf Linnemann[f], Dong Ren[g,*], Olivier Béthoux[h,i]

[a] Museum für Naturkunde Chemnitz, Moritzstraße 20, D-09111, Chemnitz, Germany
[b] TU Bergakademie Freiberg, Institut für Geologie, Bernhard-von-Cotta-Straße 2, D-09596, Freiberg, Germany
[c] Kazan Federal University, Institute of Geology and Petroleum Technologies, Kremlyovskaya 18, 420008, Kazan, Russia
[d] Institute of Geological Sciences, National Academy of Sciences of Ukraine, O. Gonchar Street 55-b, 01601, Kiev, Ukraine
[e] Museum für Naturkunde der Humboldt-Universität zu Berlin, Invalidenstraße 43, 10115, Berlin, Germany
[f] Senckenberg Naturhistorische Sammlungen Dresden, Museum für Mineralogie und Geologie, Sektion Geochronologie, Königsbrücker Landstraße 159, D-01109, Dresden, Germany
[g] College of Life Science, Capital Normal University, Beijing, 100048, China
[h] CR2P (Centre de Recherche en Paléontologie – Paris), MNHN – CNRS – Sorbonne Université, Paris, France
[i] Muséum National d'Histoire Naturelle, 57 rue Cuvier, CP38, F-75005, Paris, France

ARTICLE INFO

Keywords:
Taphonomy
Late Carboniferous
Conodonts
Ammonoids
U–Pb dating
Interdelta bay

ABSTRACT

The Early Pennsylvanian Xiaheyan entomofauna (Ningxia, China) is among the earliest assemblages of winged insects known so far, and therefore provides an essential input on deciphering the early diversification of this group. Despite its evolutionary significance, both the age and depositional environment remained poorly constrained. Here, we present high-resolution documentation of litho- and biofacies, biostratigraphy and geochronology of the up to 100 m thick type section. Accordingly, the insect-bearing strata are of latest Bashkirian (latest Duckmantian) to middle Moscovian (Bolsovian) age. The sediments, lithostratigraphically assigned to the Yanghugou Fm., represent a regressional marine sequence formed at the southern margin of the Qilian Inland Sea. Intercalations of crevasse channels and splays that laterally interlock with marine black shales and bioclastic limestones point to deposition in an interdelta bay. Ground-touching waves provoked the erosion of muds at shallow depths leading to mass mortalities among mollusc communities due to rising anoxia, turbidity and water turbulence. In addition, bottom currents transported mud intraclasts towards the basin, where sinking insects that reached the bay via winds and surface currents were buried sub-contemporaneously with bivalves below the storm wave base. Observed differences in insect preservation and assemblage composition across the sequence are found to correlate with lithology and are best explained by distance from land, and the action of events inducing insect carcasses to sink, such as storms. The proposed taphonomic model represents a new fossilization pathway from land to sea and provides new directions for prospecting Paleozoic deposits in the search for insects.

1. Introduction

Terrestrial ecosystems of the Carboniferous were characterized by an unprecedented diversity of arthropods (Dunlop, 2010; Shear and Edgecombe, 2010; Wolfe et al., 2016). As for winged insects, they make an apparent sudden appearance in the Late Mississipian (Brauckmann and Schneider, 1996; Petrulevičius and Gutiérrez, 2016). But it is not until the Early Pennsylvanian that a few suitable outcrops, such as Hagen-Vorhalle (Germany), Mazon Creek (USA) and Commentry (France) yield diverse assemblages of winged insects (Brongniart, 1893; Carpenter, 1997; Brauckmann et al., 2003). Considering the occurrence of wingless hexapods in the Devonian, the 35-million-years-long gap is most likely due to a lack of suitable outcrops. As a consequence, Early Pennsylvanian localities providing insects are of utmost importance for our understanding of the early diversification of the group.

About two decades ago fossil insects were mentioned by Hong and Peng (1995) at the Pennsylvanian Xiaheyan locality. In the last six years, this North Chinese locality was subjected to intensive excavation.

* Corresponding author.
** Corresponding author. Museum für Naturkunde Chemnitz, Moritzstraße 20, D-09111, Chemnitz, Germany
E-mail address: rendong@cnu.edu.cn (D. Ren).

https://doi.org/10.1016/j.palaeo.2019.109444
Received 27 January 2019; Received in revised form 13 October 2019; Accepted 1 November 2019

The description of the insect content is ongoing, but it can already be assessed that at least seven insect orders are present, with stem-relatives of Orthoptera (grasshoppers, crickets and katydids) dominating in terms of abundance and number of species (Prokop and Ren, 2007; Béthoux et al., 2011; Béthoux et al., 2012a,b; Li et al., 2013a,b; Wei et al., 2013; Pecharová et al., 2015; among others). Besides this remarkable diversity, the collected material is abundant, allowing solid inferences on wing venation intra-specific variability in various lineages (Béthoux et al., 2011, 2012b; Cui et al., 2011; Gu et al., 2011; Li et al., 2013; Pecharová et al., 2015), and the identification of both males and females for some species (Pecharová et al., 2015; Du et al., 2016). Moreover, the sediment preserved minute sensory structures of the insects (Prokop et al., 2016). Particularly unusual among insect-bearing Paleozoic localities is the occurrence in a thick marine black-shale succession providing abundant ammonoids and bivalves (Lu et al., 2002). Finally, insect assemblages occur in distinct layers, and it has already been shown that their composition and the state of preservation of the contained insects vary across the section (Robin et al., 2016).

However, further progress in the investigation of the Xiaheyan entomofauna is impeded by three main obstacles. First, the sampled layers are not correlated, this situation precluding a proper analysis of lateral variations in insect assemblages. Second, both depositional environment and insect taphonomy are not understood with sufficient details, making comparisons between assemblages across the section, and with other Pennsylvanian localities, weakly informative. Finally, the age of the locality remains poorly constrained.

In order to address these issues, we carried out a detailed bed-by-bed documentation of the insect-bearing strata, including correlation between the sampled areas. In addition, based on lithofacies and biofacies analysis, a detailed interpretation of the depositional environment and insect taphonomy is proposed. The age of the locality is newly assessed based on multiple proxies.

2. Geological background

The study area is located at the foothills of the eastern North Qilian Mountains, 8 km southwest of Zhongwei, Ningxia Hui Autonomous Region, in Northwest China (Fig. 1A and B). Steeply inclining strata of Pennsylvanian to early Permian age are exposed along the Xiangshan-Tianjinshan Fault — a major regional fault by which the late Paleozoic strata have been overthrusted on Cenozoic conglomerates since the Miocene (Fig. 1C; Zhang et al., 1990; Shi et al., 2015). Insect-bearing strata were considered of earliest Pennsylvanian (Namurian B/C) age based on ammonoids and conodonts (e.g., Lu et al., 2002). However, this stratigraphic affiliation remains highly controversial because of irreproducible profile documentations and a disputable regional lithostratigraphic subdivision of the Carboniferous (see Supplementary material 1).

The Ningxia region belongs to the western Sino-Korean Craton which, during the Carboniferous, was part of a tropical archipelago located at the eastern margin of the Paleo-Tethys (Fig. 2A; Nie, 1991; Wang and Pfefferkorn, 2013; Xiao et al., 2013). The Sino-Korean Craton was surrounded by passive continental margins against the Paleo-Tethys to the West and South and the Panthalassa Ocean to the East. To the North, an active andinotype volcanic arc probably marked the border to the Paleo-Asian Ocean (Shen et al., 2006; Zhang et al., 2007; Zheng et al., 2014). In relation to its paleogeographical position, Northern China underwent a tropical ever-wet climate favoring extensive coal formation from the Carboniferous until the late Permian (Liu, 1990; Cope et al., 2005). During Early Pennsylvanian times, the Ningxia region was captured by the epicontinental Qilian Basin, in which shallow marine, littoral and paralic sediments were deposited (Fig. 2B; Tong, 1993; Liu et al., 2014). According to Tong (1993) and Xie et al. (2004) the outline, internal structure and sedimentation of this basin were determined by reactivated faults.

3. Materials and methods

As a preliminary remark, materials used for lithological and geochronological analyses are stored with the inventory number FG-680 in the central sample archive (Lithothek) of the Technical University Bergakademie Freiberg, Germany. Insects used for taphonomy are housed at the Capital Normal University in Beijing/China. Each surveyed specimen is associated with a 'collect label' indicating its systematic identification, the author(s) of the identification, the name of the collector, the year of collect, and the excavation site it was recovered from. Specimens of particular importance were incorporated to the CNU-NX1 collection (together with their 'collect label'). If so, a twin of the 'collect label', on which the CNU-NX1 number is indicated, was kept together with the original, remaining sample.

3.1. Lithofacies analysis

During two field campaigns in 2014 and 2015 lithofacies, thicknesses, fossil content and taphonomy of four sections in non-disturbed areas of the Xiaheyan locality were documented at a centimetric resolution. The sections are exposed in N–S-trending erosional gullies dissecting the foothills of the North Qilian Mountains (Fig. 1B). Three sections have a length of 100 m and one has a length of 300 m with the Xiangshan-Tianjinshan Fault as its base. Lateral distance between outermost sections reaches an extent of 770 m. Stratigraphic correlation rests upon marker horizons, i.e., ash layers, carbonates or black shales showing recognizable fossil contents, and the cyclic constitution of the sections. Lithofacies analysis follows the hierarchical concept proposed by Miall (1996) in a modified form. Accordingly, sediments are grouped into lithofacies types (LFT's) defined by their texture, bedding and fossil content. Each LFT is indicated by two letters: the first, capital letter accounts for the dominating grain size, while the second, small letter indicates the bedding (Table 1). Additionally, particular capital letters were applied in case of notable sedimentological features. Microfacies and petrography were characterized by means of 20 thin sections. The spatial arrangement of the LFT's is used to describe the lithofacies architectures of the Xiaheyan profile.

3.2. Insect taphonomy

Insect assemblages have been collected from several excavation sites. Their names include the name of the corresponding section plus a consecutive number indicating the chronological order of opening [e.g. the assemblage 'Peacock 0' (Pe 0) was excavated earlier than assemblage 'Peacock 1' (Pe 1), both originating from Peacock Hill section]. Taphonomic analysis follows the procedure elaborated by one of us (OB) and described in Robin et al. (2016; suppl. data). We complemented data from these authors with 166 specimens from two sites, namely Peacock 2 and Dragon 4.

3.3. Biostratigraphy and geochronology

Two fossiliferous limestone horizons were sampled and processed with 10% formic acid to extract conodont material. In addition, two out of four ash layers were sampled to obtain U–Pb ages from zircons. Zircons were analyzed for U, Th, and Pb isotopes by Laser Ablation and Inductively Coupled Plasma Mass Spectrometry (LA-ICP-MS) at the GeoPlasma Lab, Senckenberg Naturhistorische Sammlungen Dresden, using a Thermo-Scientific Element 2 XR sector field ICP-MS coupled to a RESOLUTION Excimer Laser System (193 nm). For further detail on geochronology, see Supplementary material 2.

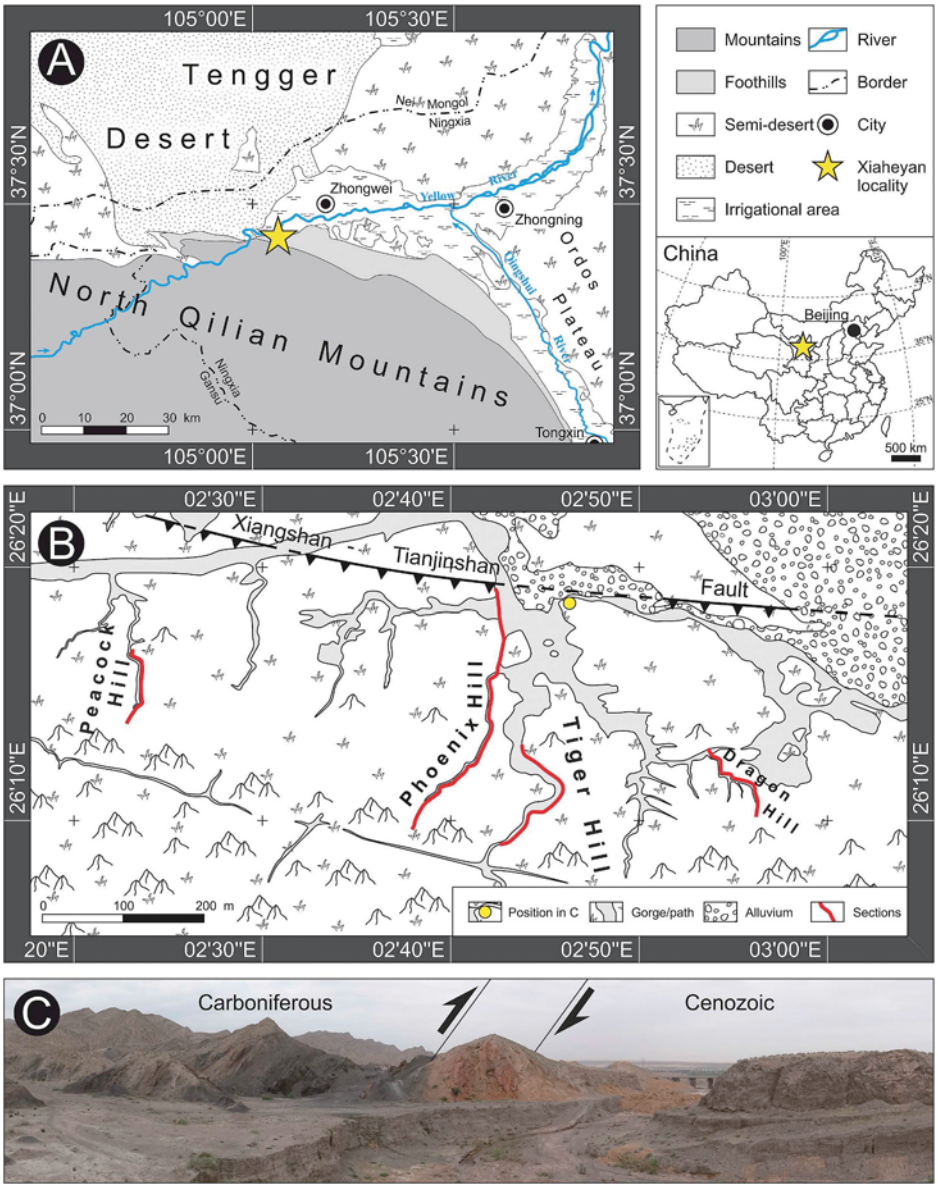

Fig. 1. Xiaheyan locality. (A, B) Position of the study area in the Ningxia Province (China). (C) View at the Xiangshan-Tianjinshan Fault, which separates steeply inclining Carboniferous strata in the south from horizontal Cenozoic conglomerates in the north.

4. Results

4.1. Lithofacies types

Generally, the Xiaheyan sections are composed of two facies: a prevailing black shale facies with subordinate carbonates and a clastic non-shale facies. Whereas the clastic non-shale LFT's are summarized in Table 2 and Fig. 3, the insect-bearing black shale facies is described in detail in the following.

Four LFT's can be distinguished within the black shale facies. One is dominated by horizontal lamination (LFT Bh), two show a fabric referred to as lenticular lamination (O'Brian and Slatt, 1990; Schieber et al., 2010, Fig. 4A and B), and one is massive (LFT Bm). Focusing on lenticular lamination, the fabric consists of an accumulation of (sub-) mm-scale ellipsoidal mud aggregates, each exhibiting a lenticular to irregular shape in vertical sections (Figs. 4A and B). Lenticularly laminated LFT's differ in size of the mud intraclasts and include intercalations of 1 mm thick, non-stratified siltstone layers, delimitated by sharp lower and upper boundaries (Fig. 4C). Micro cross-lamination is rarely evident (Figs. 4C and D). Up to 300 µm large angular to rounded quartz grains can occur (Fig. 4E). Around quartz grains as well as shell remains, the sediment is differentially compacted (Figs. 4E and F).

4.1.1. LFT Bh: horizontally laminated black shale (Fig. 4G and H)

Black shales of LFT Bh possess horizontal bedding that consists of 250–300 µm thick horizontal laminae showing sharp boundaries (Figs. 4G and H). In a vertical direction, laminae may change in their internal structure, ranging from laminae transitional to LFT Bl_2 to laminae showing inverse grading (both shown in Fig. 4G). Intercalations of LFT Bl_2 layers are common. Fossils are extremely rare, including insect remains, the bivalve *Posidoniella* de Koninck, 1885, indeterminable juvenile molluscs and plants. Among the latter, highly macerated fragments as well as up to 10 cm large lycopsid stems, sphenopsid and pteridosperm foliages were found.

4.1.2. LFT Bl_1: lenticularly laminated black shale 1 (Fig. 5)

This macroscopically light greyish LFT consists of tightly packed mud aggregates ranging in size from 75 to 170 µm in vertical diameter, and from 250 to 1500 µm in horizontal diameter (Fig. 5A). The fossil content is dominated by low-diversity bivalve mass assemblages,

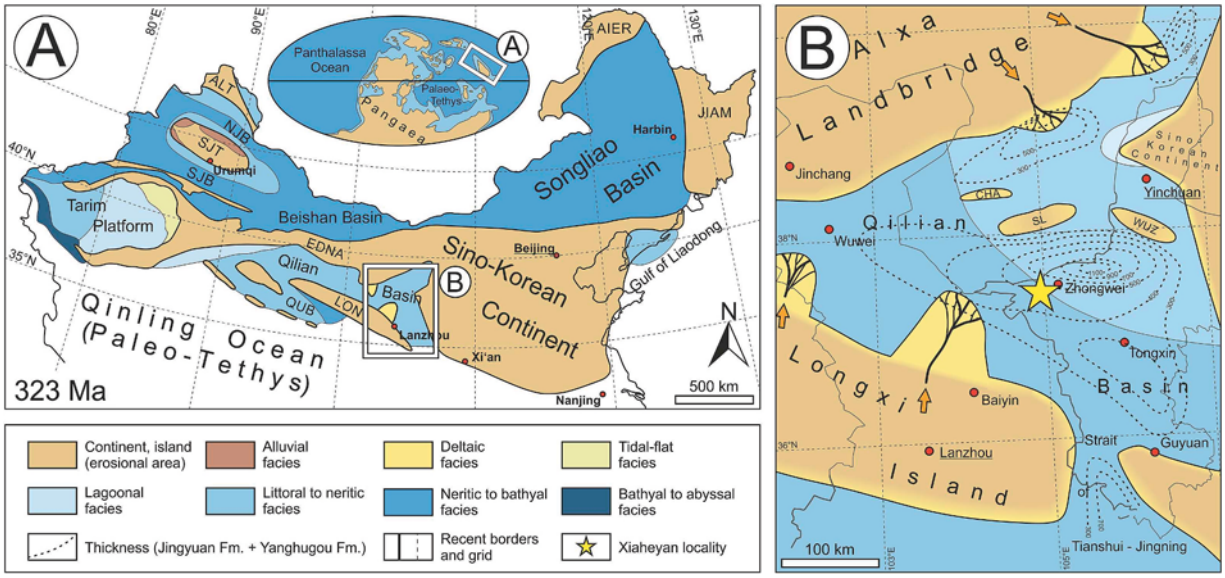

Fig. 2. Paleogeography of Northern China (A) and Ningxia (B) around the Mississippian-Pennsylvanian boundary. Compiled and modified after Tong and Li (1994), Ruan (1996), Zhu et al. (2007) and Yan et al. (2008). Abbreviations: AIER: Aierguna Island; ALT: Altai Island; EDNA: East Tarim-Dunhuang-North Qilian-Alxa Land bridge; JIAM: Jiamusi Island; LON: Longxi Island; NJB: North Junggar Basin; QUB: Quaidam Basin; SJB: South Junggar Basin; SJT: South-Junggar-Tuha Island.

Table 1
Symbology used for lithofacies analysis.

Grain size	Bedding	Special symbols
G Gravel	b lenticularly bedded	B Black shale
S Sand	g graded	C Coaly mud
F Fine-clastics	h horizontally bedded	L Limestone
	l lenticularly laminated	R Rooted siltstone
	m massive	
	r ripple-cross bedded	
	t trough-cross bedded	

including complete juvenile and adult specimens, lacking orientation and sorting (Fig. 5B). Butterfly preservation remains an exception. Instead, most specimens have their valves still occluded. The shell beds mainly consist of *Posidoniella* (Fig. 5C), reaching a maximum size of 5 cm, followed by *Dunbarella* Newell, 1938 (Fig. 5D). Adult *Euchondria* Meek, 1874 (Fig. 5E) and assemblages exclusively composed of mytiloids (Fig. 5G) occur sparsely. Cm-scale plant remains can be surrounded by sparse to dense accumulations of juvenile *Posidoniella* individuals (Fig. 5F). In this case, most individuals have their umbo orientated towards the plant – often with the umbo in connection with

Table 2
Non-shale lithofacies types.

Facies code	Facies description (incl. figure reference)	Interpretation
C	Black, coaly mudstones with faint horizontal bedding and tiny plant remains. Occurs rarely and forms a few centimeters thick horizons (Fig. 3A).	Standing water body with high accumulation rate of organic matter.
R	Greyish brown siltstones with indistinct horizontal bedding. Subhorizontally penetrated by abundant, 2–6 mm thick roots resembling lycopsid appendices, which may increase in size towards the top (Fig. 3B).	Autochthonous incipient root soil.
Fh	Brown siltstones with horizontal bedding. Bedding planes are covered by mica and tiny plant remains preserved as compressions. Rare intercalations of dense accumulations of up to 10 cm large lycopsid stems and pteridophyte fronds (Fig. 3C).	Subaquatic deposition at low-energetic, unidirectional flow conditions.
Sb	Greyish white fine- to medium-grained silty sandstones with lenticular bedding. Primary fabric often obliterated by soft-sediment deformation (Fig. 3D).	Subaquatic deposition at fluctuating low-energetic, unidirectional flow conditions.
Sr	Greyish yellow fine- to medium-grained sandstones with ripple-cross bedding on a 0,5 cm-scale (Fig. 3E).	Subaquatic deposition of the lower flow regime.
Sh	Greyish white well-sorted fine-grained sandstones showing horizontal lamination on a mm-scale (Fig. 3F).	Subaquatic deposition at high stream velocities (upper plane bed).
St	Grey, pebbly, moderate- to coarse-grained sandstones showing small- to medium-scaled through-cross bedding (i. e. sets of less than 20 cm in thickness) (Fig. 3G).	Subaquatic dunes of the lower flow regime.
Sg	Poorly sorted, pebbly fine- to medium-grained sandstones with a sharp erosional base. Pebble fraction consists of rounded to subrounded quartz and irregularly shaped, often flattened black shale clasts at maximum diameters of 4 cm. The black shale clasts are orientated subhorizontally and decrease in size and abundance towards the top of lithofacies type Sg reflecting a normal grading. Occurrence of coalified, tiny plant remains (Fig. 3H).	Event-like deposition of hyperconcentrated to mass flows including the reworking of still plastic black shales.
Sm	Poorly sorted, pebbly fine- to coarse-grained massive sandstones. Quartz grains rounded to subrounded. Base and top are uneven, but sharp (Fig. 3I).	Subaquatic mass flow events.
Gm	Non-stratified, sandy, fine-grained conglomerates. Matrix cemented by calcite with (sub) angular grains. Pebble fraction rounded to subrounded. High compositional maturity with quartz as only component (Fig. 11J).	Highly energetic, subaquatic mass flows.

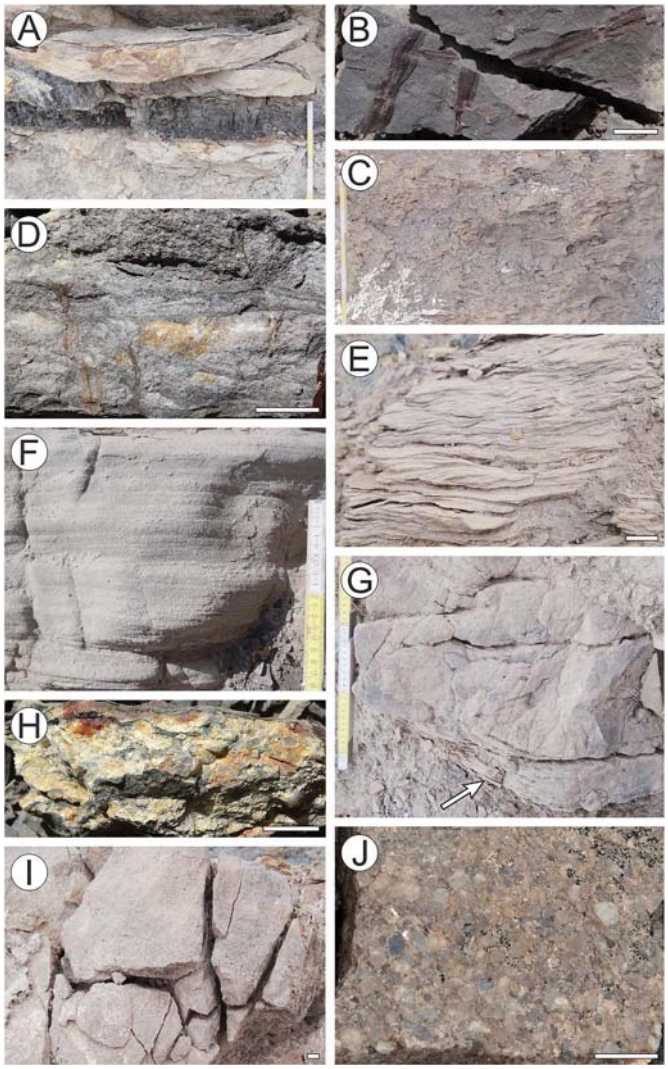

Fig. 3. LFT's of the non-shale facies. Scale: 1 cm. (A) LFT C represented by a coal seam underlain by a rooted soil and overlain by trough-cross bedded sandstones. (B) LFT R with lycopsid appendices on a bedding plane in siltstones. (C) LFT Fh. (D) LFT Sl. (E) LFT Sr. (F) LFT Sh. (G) LFT St. Note incision into underlying fine-clastics (arrow). (H) LFT Sg. (I) LFT Sm. (J) LFT Gm.

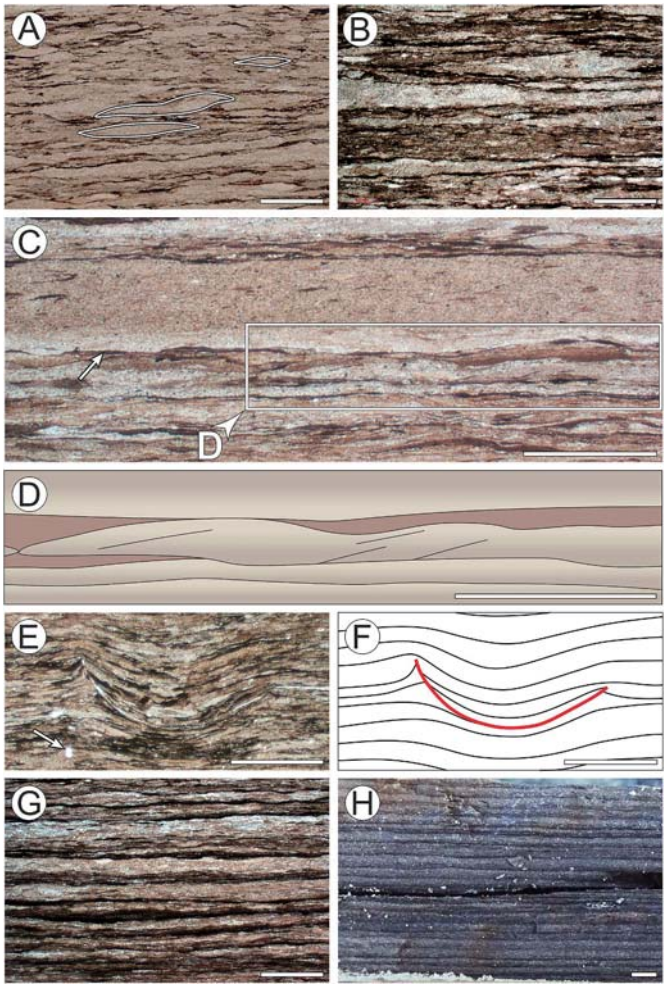

Fig. 4. Black shale microfabrics. Scale: 1000 µm. (A, B) Lenticular shape of mud aggregates (lines) in sections vertical to bedding. (C) Intercalation of a non-stratified siltstone layer, interpreted as distal turbidity current deposit. Note sharp boundaries (arrow). (D) Schematic close-up of C showing micro-cross stratification. (E, F) Differential compaction around a shell (red line in D). Note detrital quartz (arrow). (G, H) Microfacies (cross-cut) of LFT Bh. Note the distinct horizontal lamination. (For interpretation of the references to color in this figure legend, the reader is referred to the Web version of this article.)

the plant itself. Some bedding planes display patchy accumulations of up to 3 mm large juvenile molluscs, displaying a discoid shape and a central cavity (Fig. 5H). Further relevant fossils are fragmentarily to completely preserved ammonoids (Fig. 5I), at least 3 cm long orthocone nautilids preserved as molds (Fig. 5J), a tealliocaridid crustacean (*Laevitealliocaris xiaheyanensis* Yang et al., 2018), insect remains and fish scales. Plant fossils comprise lycopsid and sphenopsid foliages (*Lepidophylloides* Snigirevskaya, 1958, *Sphenophyllum* Brongniart, 1828, Fig. 5K, *Annularia* Sternberg, 1821), stems, single neuropterid leaflets, and plant fragments too incomplete and/or poorly preserved for proper systematic identification.

4.1.3. LFT Bl_2: lenticularly laminated black shale 2 (Fig. 4B)

On exposed surfaces, the greyish LFT Bl_2 is covered by secondarily formed jarosite and oxyhydroxides (Odin et al., 2018). Internally, tightly packed mud aggregates reach vertical diameters of 90–500 µm, as opposed to horizontal diameters of 500 µm to a couple of mm (Fig. 4A). The fossil content in general is identical to that of LFT Bl_1, although it lacks mass occurrences of shells. Assemblages are characterized by sparse but more balanced accumulations of bivalves (*Posidoniella*, *Dunbarella*), complete and fragmentary ammonoids, juvenile molluscs, insects and plant fragments. Monospecific accumulations are rare and dominated by bivalves. In contrast to LFT Bl_1, plant remains are larger and more diverse, containing tiny fragments, sphenopsid and lycopsid stems and foliages, neuropterid leaflets, pteridosperm fronds and cordaitalean leaves.

4.1.4. LFT Bm: massive black shale (Fig. 6)

This LFT represents pure to silty black-colored claystone accounting for approximately one half of each Dragon, Phoenix and Peacock Hill sections. Due to the almost uniform grain size, a lumpy breakage is more common than cleavage along the bedding planes. At a microscopic scale, dark homogeneous clay dominates, rarely interspersed with up to 50 µm thick silt aggregates (Fig. 6A). This LFT is commonly associated with calcite or siderite intercalations, decimeters to 6 m long and up to 50 cm thick, and arranged in distinct stratigraphic levels (Fig. 6B). Spacing of bedding planes in the enveloping claystones increases towards these carbonates (Fig. 6C), indicating an early diagenetic origin.

Horizons with *Planolites* Nicholson, 1873 sporadically occur (Fig. 6D). Fossils are rare and comprise strongly macerated plant remains and isolated neuropterid pinnulae, rare and partially articulated

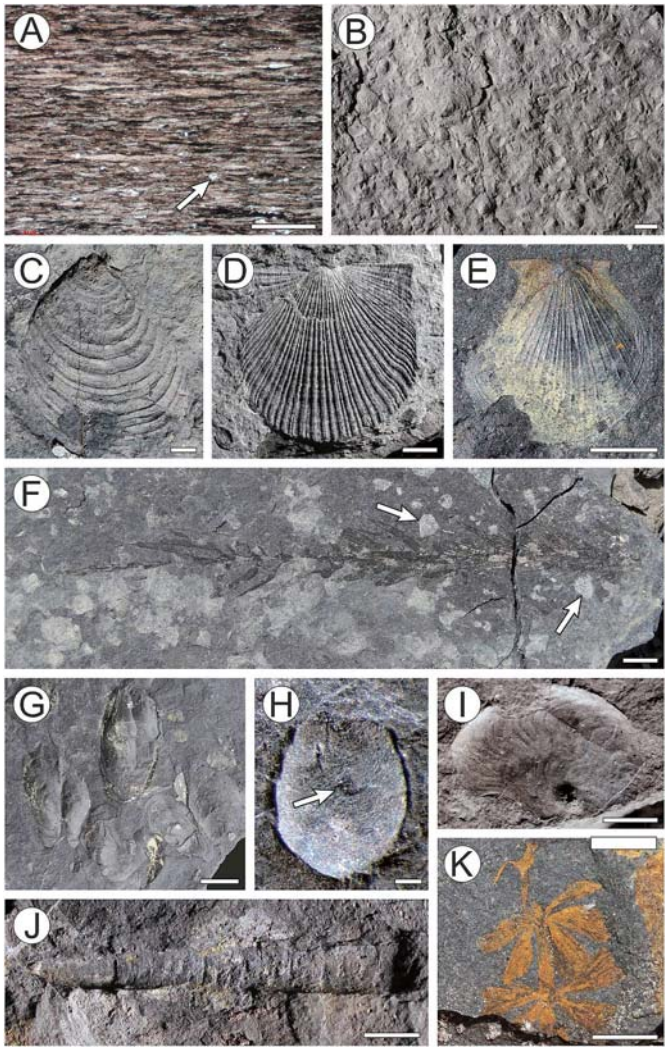

Fig. 5. LFT Bl_1. (A) Microfacies (cross-cut). Note fine quartz sand grains (arrow). Scale: 1 mm. (B) Accumulation of juvenile *Posidoniella* shells on bedding plane. Note different sizes and the missing orientation of specimens. Scale: 5 mm. (C) *Posidoniella* de Koninck, (1885). Scale: 5 mm. (D) *Dunbarella* Newell, (1938). Scale: 5 mm. (E) *Aviculopecten* McCoy, (1851). Scale: 5 mm. (F) Lycopsid sprout accompanied by sparse and dense clusters of juvenile *Posidoniella* specimens. Note the orientation of the umbo towards the plant (arrows). (G) Mytiloid shells in butterfly preservation. Scale: 5 mm. (H) Close-up of indeterminable juvenile mollusc showing a central cavity (arrow). Scale: 2 µm. (I) Ammonoid fragment. Scale: 5 mm. (J) Orthocone nautilid preserved as a mold. Scale: 5 mm. (K) *Sphenophyllum* sp., imprint coated with limonite. Scale: 5 mm.

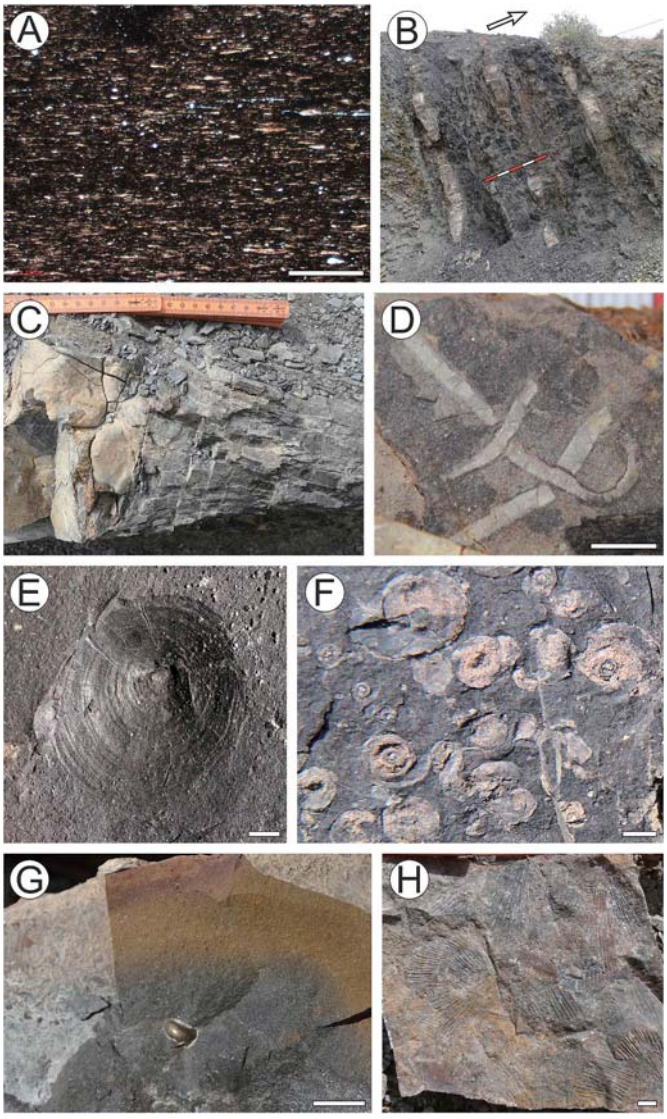

Fig. 6. LFT Bm. (A) Microfacies (cross-cut) showing rare silt aggregates in a claystone matrix. Scale: 1 mm. (B) Early diagenetic limestone concretions. Scale: 50 cm. The black arrow points to the top. (C) Close-up of B proving differential compaction of black shales. (D) *Planolites* tubes on bedding plane. Scale: 5 mm. (E) Lingulid brachiopod *Orbiculoidea* d'Orbigny, (1847) . Scale: 1 mm. (F) Complete and fragmentary ammonoid tests of different ontogenetic stages on a bedding plane. Scale: 5 mm. (G) Gastropod whorl preserved as pyritized steinkern in a sideritic concretion. Scale: 5 mm. (H) Dense accumulation of *Dunbarella* on a bedding plane within a calcitic concretion. Scale: 5 mm.

to isolated remains of actinopterygiid fish, lingulid brachiopods (*Orbiculoidea* d'Orbigny, 1847, Fig. 6E) and bivalves (*Dunbarella*, *Posidoniella*). In places, mass occurrences of complete and fragmented juvenile and adult ammonoids together with sparse plant fragments occur (Fig. 6F). Siderite concretions rarely contain accumulations of tiny shells and gastropods (Fig. 6G). The fossil content of calcite concretions ranges from dense, up to 20 cm thick, monospecific accumulations of *Dunbarella* (Fig. 6H) to oligospecific, dispersed assemblages made up of ostracods, gastropods and ammonoids (in decreasing order of abundance).

4.1.5. LFT Lg: graded to stratified limestone (Fig. 7)

This LFT forms up to 40 cm thick beds (Fig. 7A) that can be traced laterally across distances of at least 1 km. Microscopically, they range from mudstones to floatstones and packstones made up of peloids showing average grain sizes of 200 µm (max. 625 µm), coarse silt to sub-rounded quartz fine-sand and skeletal components (Figs. 7B and C). Fossils comprise ostracod valves, crinoid columnal segments, complete juvenile ammonoids and gastropods, isolated valves and tiny shell fragments in variable proportions. Beds of LFT Lg are subdivided into a lower unstratified part, with roughly aligned or nested components, and an upper part, bedded horizontally to wavily, in which components are orientated parallel to bedding (Figs. 7D and E). Horizontally aligned ostracod and mollusc valves occur both in convex-up and convex-down positions.

4.2. Section structure and facies architectures

4.2.1. Thickness and cyclicities

The 350 m thick Xiaheyan section is subdivided into four units (Fig. 8; for legend see Fig. 9). The lower 90 m thick unit 1 consists of

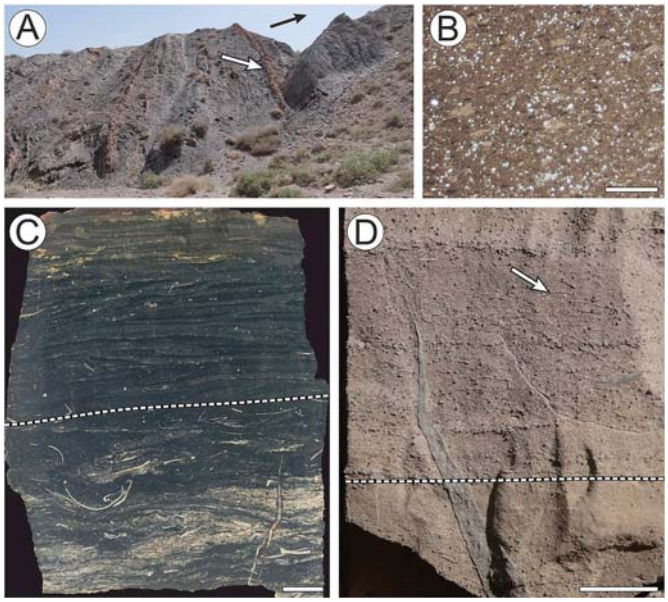

Fig. 7. LFT Lg. (A) Upper part of unit 3 at Tiger Hill (view towards East) revealing limestone banks (arrow). Black arrow pointing to the top. (B) Massive sandy pelmicrite at the base of LFT Lg. Scale: 1 mm. (C, D) Cross sections of LFT Lg. Note normal grading and horizontal alignment (arrow) of skeletal components and the transition (dashed line) from a lower, weakly stratified part to an upper, wavily or horizontally stratified part. Scale: 1 cm.

black shales and rare carbonates. It is overlain by the 80 m thick unit 2 containing black shales only (for detailed documentation see Supplementary material 3). Unit 3 has a thickness of 101 m at Dragon Hill and decreases westwards (86 m at Phoenix Hill, 78 m at Peacock Hill; Figs. 8 and 10). It begins with a coarse-clastic intercalation followed by black shales including carbonates and the insect-bearing strata. The section ends with the 80 m thick unit 4 composing of brown to pale siltstones and through-cross bedded sandstones.

The unit 3 displays repeated patterns indicative of a cyclic origin. Symmetrical and asymmetrical cycles of three orders were detected (Fig. 10). Third-order cycles are evidenced by the symmetric alternation of LFT Bm and laminated black shales (LFT's Bl_1, Bl_2, Bh) on a 1- to 3-m scale. Transitions always remain gradual. Third-order cycles can be traced laterally across distances of at least 1 km.

In an upward direction, within third-order cycles, the proportion of laminated black shales increases at the expense of LFT Bm. This repetition composes the cyclicity of second order (Fig. 10). Accordingly, each of the 15–28 m thick second-order cycles typically begins with a thick LFT Bm unit (e.g., Dragon Hill, beds 49–51; Peacock Hill, beds 24–27; Fig. 10). Laminated black shales (LFT's Bl_1, Bl_2, Bh), in contrast, dominate the upper part. Second-order cycles additionally reveal an upward-coarsening of black shale lamination, with LFT Bl_1 prevailing in the lower part and LFT BL_2 characterizing the upper part of a cycle (Fig. 10). If present, LFT Bh typically forms the topmost bed of a second-order cycle.

Finally, an upward-increasing content and thickness of LFT Bh beds at the top of second-order cycles composes the first-order cyclicity (Fig. 10).

4.2.2. Crevasse channels and splays

Crevasse channel elements occur in the basal part of unit 3 (Fig. 10), where they form lens-shaped, 10–150 m wide and less than 10 m thick bodies embedded in black shales of LFT Bm (Fig. 11A). Neighboring elements can be laterally connected by a thin sandstone layer made up of the LFTs Sl and Sh, or they are separated by black shales (Fig. 10E). Except for Peacock Hill, in which sandstones occur at a higher level (Fig. 10), crevasse elements are arranged in the same stratigraphic level at Dragon, Tiger and Phoenix hills. These deposits occur at the top of second-order cycles (Fig. 10).

Internally, larger crevasse channel elements possess a tripartite structure (Fig. 11A): the channel proper occupying the middle part is flanked by a levee facies on both sides. The channel proper facies is composed of stacked, small- to medium-scaled trough-cross bedded sandstones (LFT St, Fig. 11C) cutting erosively into the underlying black shales (Fig. 3G). To the top, a succession of LFT Sr, LFT R, and marine black shales (LFT Bm) reflects a fining-upwards. The lithologically more heterogeneous levee facies shows an interfingering of marine black shales and sheet-like non-shale LFT's, such as massive sandstones (Sm), autochthonous root soils (R), and coaly claystones (C), indicating subaerial deposition. In root soils, dm-scale channel elements composed of LFT Sr (Figs. 11A, B, D, F) occur. Crevasse splays are recorded by discrete sheet-like intercalations of the LFT's Sr or Gm being a few decimeters thick and less than 400 m wide (Figs. 11A, G-I; Elliot, 1974). Both the base and top are sharp and even (Fig. 11G), the former being accompanied by abundant reworked *Stigmaria* fragments in case of conglomeratic deposits (Figs. 11H and I). Bleaching of black shales can be present down to a depth of a few decimeters beneath crevasse splay and channel sediments (Fig. 11F).

4.3. Insect taphonomy

4.3.1. Assemblages composition

Generally, archaeorthopterans (i.e. stem-Orthoptera) dominate all insect assemblages, with ratios ranging from 63 to 74% (Fig. 12A). The assemblages from Phoenix 0 and Peacock 2 are dominated by two species belonging to this group. In contrast, assemblages from Dragon 4 and Phoenix 2 display a more balanced composition, in particular the latter, in which six species each account for ca. 10–13% of the whole assemblage.

4.3.2. Relation of preservation and lithology

Depending on the embedding black shale LFT's, insect assemblages differ considerably in terms of preservation. In the Phoenix 0 assemblage, embedded in LFT Bh, the content of at least partially articulated specimens reaches a value of more than 95% (Fig. 12B). About a third of neopteran individuals display wings in a resting position (Fig. 12C). As for abdomen preservation (Fig. 12D), intact ones predominate (ca. 60%). The loss of abdomen prior to burial represents a minor fraction (20%).

Compared to Phoenix 0, assemblages from LFT Bl_2 (Peacock 2, Dragon 4), which are also deeper in the sequence, have fewer wings that are at least partially articulated (70–80% of assemblages; Fig. 12B). Having wings in a resting position is rarely present among the recovered neopterans (Fig. 12C). The type of preservation of the abdomen differs between the two sites (Fig. 12D). However, even though the Peacock 2 assemblage resembles that from Phoenix 0, comparison with that recovered from Dragon 4 is uneasy, as only four specimens for which abdominal preservation can be assessed were recovered from the latter. Indirectly, this suggests that Dragon 4 represents an assemblage of specimens more altered than at Peacock 2.

Finally, the assemblage from Phoenix 2 (LFT Bl_1), which is the most basally located in the sequence, is dominated by isolated wings (Fig. 12B), in sharp contrast with the three other sites. Among the few neopteran specimens providing information on wing orientation, more than 90% have their wings variously spread (Fig. 12C). As for Dragon 4, because partially articulated (leave alone complete specimens) are extremely rare, abdominal preservation remains an exception, and therefore can barely be evaluated (Fig. 12D).

4.4. Relative and absolute data for stratigraphic correlation

4.4.1. Conodonts and goniatites

Processing of selected carbonate beds (units 6 and 36 at Peacock Hill; Fig. 10) delivered two dozens of complete and fragmentary conodonts. In general, assemblages are dominated by P1 elements (Figs. 13A–N, S) followed by ramiform elements (Figs. 13O–R, T–V).

However, conodont assemblages differ markedly in their composition, except for *Hindeodella* elements (Figs. 13P–R, T–V) occurring in

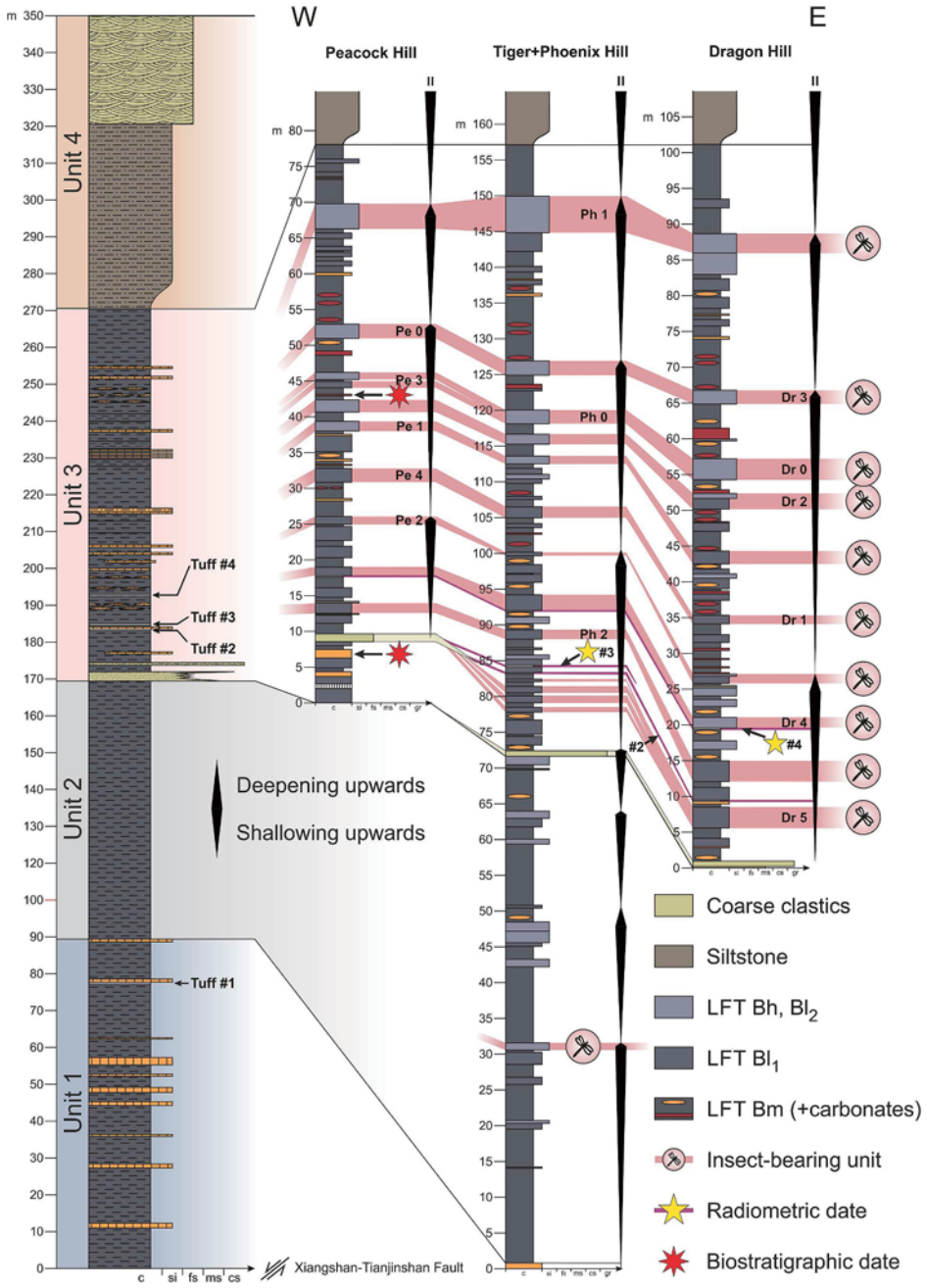

Fig. 8. Profile of the Xiaheyan section showing 14 insect assemblages gained from ten horizons. Abbreviations: Dr: Dragon. Pe: Peacock. Ph: Phoenix. For detailed legend see Fig. 9.

both limestones. In bed 6 at Peacock Hill, the genus *Declinognathodus* Ellison and Graves, 1941 prevails, and is represented by *Declinognathodus marginodosus* Grayson, 1984 (Figs. 13C, L) and several specimens with unclear species affiliation (Figs. 13A, I, S). Two of the problematic ones (Figs. 13A, S) show similarities with *Declinognathodus lateralis* Higgins and Bouckaert, 1968, as their carina turns towards one parapet without merging with it. In contrast to *D. lateralis*, in which the blade meets the platform in an axial position, the blade-platform junction of the specimens represented in Fig. 13A and 14S is more marginal, causing a bending of the carina. Besides *Declinognathodus*, one element attributable to *Neognathodus* sp. (Fig. 13J) and an M element of *Idioprioniodus conjunctus* Gunnell, 1931 (Fig. 13O) were recovered.

A well-preserved steinkern of *Gastrioceras* cf. *listeri* Sowerby, 1812 (Fig. 14) was found in bed 3 at Dragon Hill, being correlated lithostratigraphically with the conodont-bearing limestone of bed 6 at Peacock Hill. The specimen closely resembles material already published as *Gastrioceras listeri* by Ruan and Zhou (1987) and *Gastrioceras montgomeryense* Miller and Gurley (1896) by Yang (1987) from the Xiaoyuchuan locality in the North Qilian Mountains, 40 km south-east of Xiaheyan.

The conodont assemblage from bed 36 at Peacock Hill is composed of juvenile and adult *Idiognathodus* specimens (Figs. 13F, G, H, K, M, N and Figs. 13B, D; respectively). Among them, *Idiognathodus praeobliquus* Nemyrovska et al. (1999) (Fig. 13B) was found.

4.4.2. U–Pb dating

Data about tuff lithology and morphology of zircons used for isotope measurements are provided in Supplementary materials 4 and 5; raw data are summarized in Supplementary materials 6 and 7. For tuff #3, an isotopic age of 314.0 ± 3.0 Ma was asserted (MSWD: 2.6; probability of concordance: 0.11; Supplementary material 6). Tuff #4 yielded an age of 312.0 ± 3.0 Ma (MSDW: 3.1, probability of concordance: 0.079; Supplementary material 8).

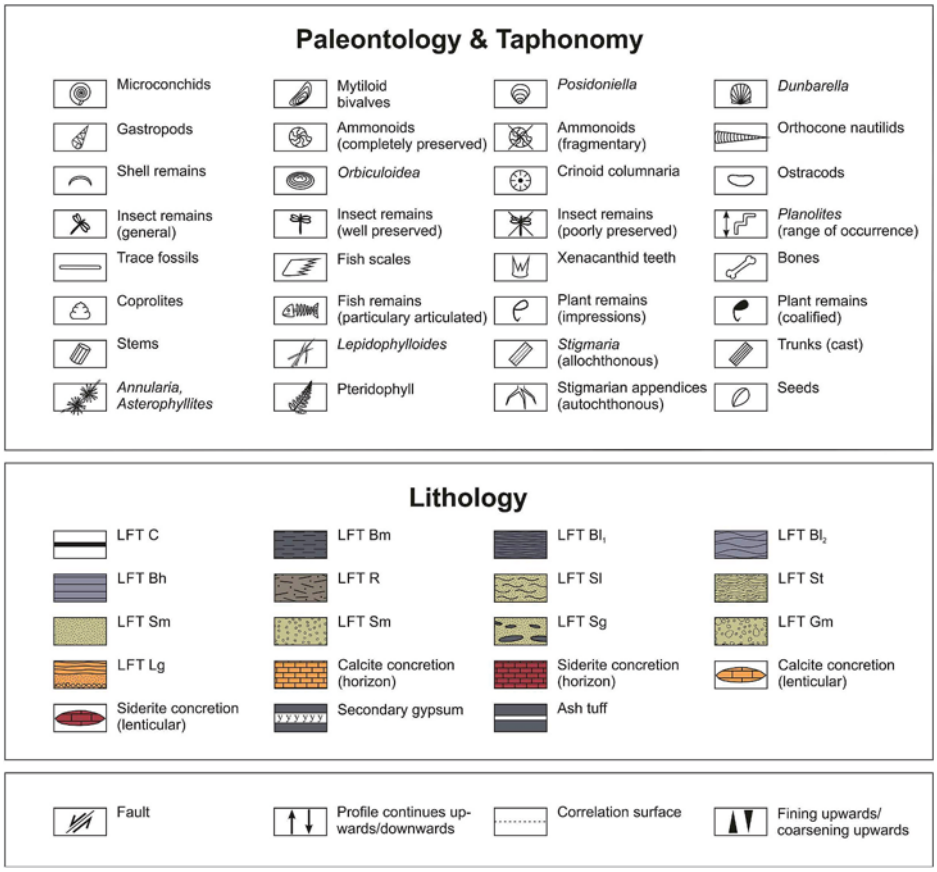

Fig. 9. Legend of signatures used in profiles.

5. Discussion

5.1. Age and stratigraphy of the Xiaheyan entomofauna

In bed 6, the conodont *Declinognathodus marginodosus* is a cosmopolitan species that defines the homonymous biozone of latest Bashkirian to earliest Moscovian age (Fig. 15; Nemyrovska, 1999; Davydov et al., 2010, 2012). This age range for bed 6 can be limited to the latest Bashkirian (Duckmantian), as plesiomorphic features (adcarinal grooves, narrow platform and parapets) of co-occurring *Neognathodus* specimens suggest (Nemyrovska, 1999). A latest Bashkirian age is additionally supported by the discovery of a specimen of *Gastrioceras* cf. *listeri* (Fig. 14) in the same bed. *Gastrioceras* species with this conch morphology (coronate shape with angular umbilical margin and coarse ribs) are representatives of the globally applicable late Bashkirian *Brannerоceras-Gastrioceras* genus zone (Davydov et al., 2012; Korn and Klug, 2015, Fig. 15). In Western Europe, the FAD of the genus *Gastrioceras* traditionally defines the base of the Westphalian (Korn, 2007).

Concerning bed 36, the conodont species *Idiognathodus praeobliquus* has been reported from the Donets and Midcontinent basins, where it indicates a middle Moscovian (Bolsovian) age (Fig. 15; Nemyrovska et al., 1999; Marshall, 2010; Nemyrovska, 2017). A post-Bashkirian age for bed 36 is also indicated by juvenile *Idiognathodus* specimens, because their prominent rostral ridges, which reach far beyond the anterior margin of the platform, appear to be too advanced for Bashkirian *Idiognathodus*.

In summary, deposition of the insect-bearing strata started in the latest Bashkirian (Duckmantian) and persisted, at least, into the middle Moscovian (Bolsovian). This biostratigraphic evaluation is consistent with the obtained isotopic ages (Fig. 15), and was already foreshadowed by systematic works on the insect content. Zhang et al. (2013), for instance, found venation patterns of the Xiaheyan stem-Dictyoptera *Qilianiblatta namurensis* to resemble Westphalian forms. However, given the presence of LFT's $Bl_{1/2}$ and Bh in unit 2, including one horizon providing insects (Fig. 8, Supplementary material 3), the insect fossil record could possibly reach back to the middle Bashkirian (Namurian C/Westphalian A). A late Moscovian or even Kasimovian age for the uppermost insect-bearing strata cannot be excluded given the fact that more than 45% of unit 3 is positioned above the uppermost sampled limestone horizon. However, the new age data invalidates a 'Namurian age' and readjusts timelines of Pennsylvanian insect evolution in Eastern Asia.

5.2. Depositional environment

Sediments of the Xiaheyan section (units 1–4) recorded the accumulation of a voluminous marine mudstone succession (units 1–3, Fig. 8) that originally possessed a larger thickness, given abundant early diagenetic limestones (Figs.6B and C). Although radiometric and biostratigraphic data are provided only for the basal part of unit 3 (Fig. 15), it can be concluded that the whole Xiaheyan section (units 1–4) was formed over a period of a few million years. In addition, the depositional system appeared to be prograding, as evidenced by coarsening-upwards cycles of various orders (parasequences in terms of sequence stratigraphy), culminating with fluvial deposits of unit 4 (Figs. 8 and 10). A prograding marine environment prone to a long-time accumulation of thick, partially laminated black shales along with the contemporaneous burial of marine and terrestrial biota is unusual.

At first glance, the aforementioned characteristics are indicative of a prodelta environment. Located at the interface of a river and the ocean, the prodelta is the major sink for the fine-grained suspension load deposited as clay and silt below the storm-wave base. However, two crucial lithological features make this reconstruction questionable.

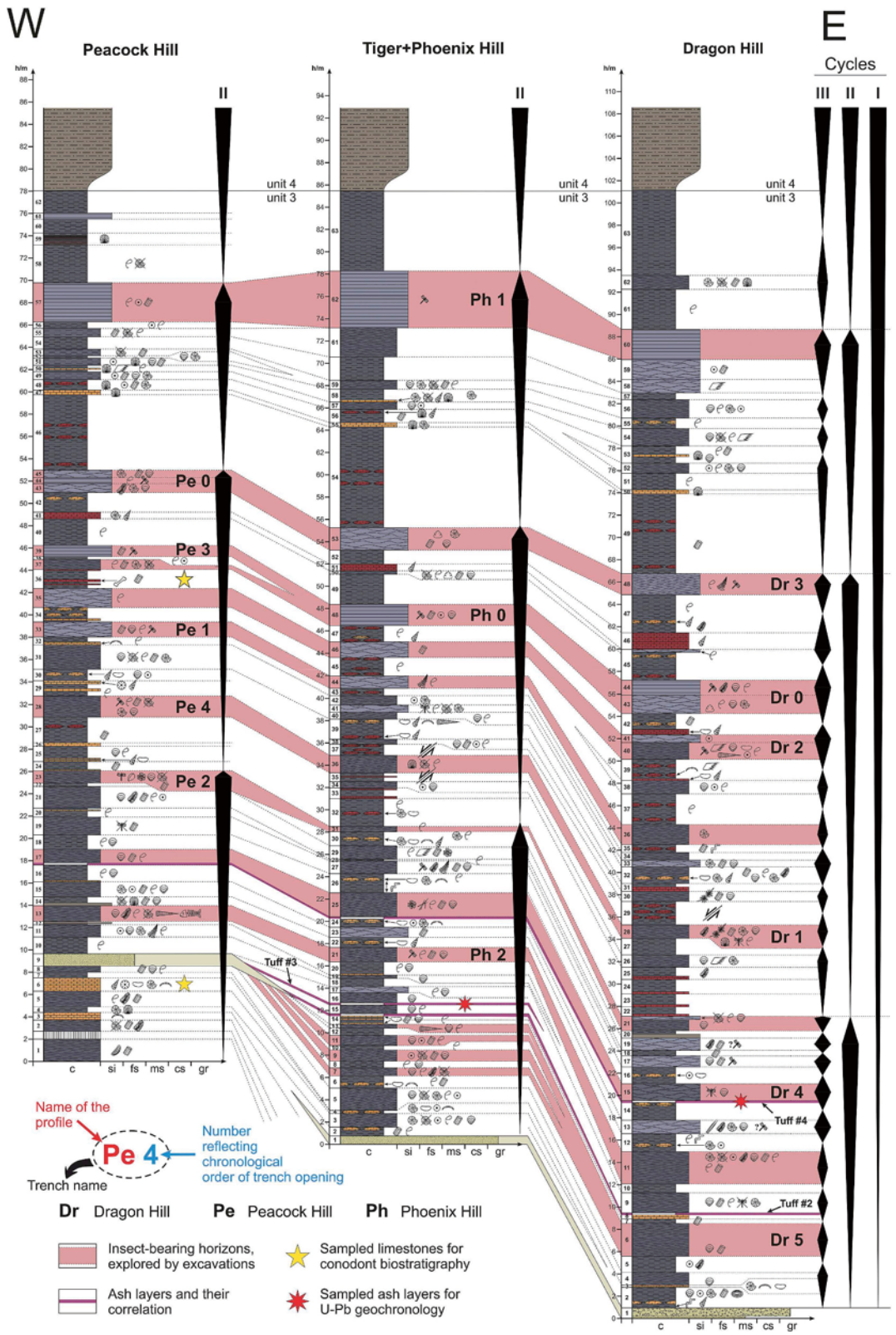

Fig. 10. Detailed profile documentation of unit 3. Note that stratigraphic occurrence of black shale LFT's reflects a cyclic constitution of the section. For legend see Fig. 9.

The first point is the presence of crevasse channel and splay deposits occurring in the basal part of unit 3 (Fig. 8). Since these subaerial to shallow-water sediments interfinger laterally with, and are overlain by black claystones of LFT Bm (Fig. 11A–F), a deep marine (i.e. prodeltaic) formation of the latter is problematic. There are two ways to address this contradiction: either crevasse deposits represent a sudden phase of sea level drop (lowstand), or black shales were formed, at least partially, at water depths shallower than initially assumed. Under the first option, the stratigraphic level of the crevasse deposits should reflect any shallowing by a change in lithology and/or incisive events (e.g.,